LEGIBILITY NOTICE

A major purpose of the Technical Information Center is to provide the broadest dissemination possible of information contained in DOE's Research and Development Reports to business, industry, the academic community, and federal, state and local governments.

Although portions of this report are not reproducible, it is being made available in microfiche to facilitate the availability of those parts of the document which are legible.

3

LA-UR-87-1980

LA-UR--87-1980

DE87 011779

Los Alamos National Laboratory is operated by the University of California for the United States Department of Energy under contract W-7405-ENG-36

TITLE: THREE-DIMENSIONAL COMPUTER MODELING OF PARTICULATE FLOW AROUND DUST MONITORS

AUTHOR(S): B. D. Nichols and W. S. Gregory

SUBMITTED TO: To be presented at the 3rd Mine Ventilation Symposium at The Pennsylvania State University on October 12--14, 1987

DISCLAIMER

Los Alamos Los Alamos National Laboratory
Los Alamos, New Mexico 87545

THREE-DIMENSIONAL COMPUTER MODELING OF PARTICULATE FLOW AROUND DUST MONITORS

by

B. D. Nichols and W. S. Gregory

Los Alamos National Laboratory
Los Alamos, New Mexico

ABSTRACT

SOLA-DM is a three-dimensional finite-difference computer code designed to model the dynamics of an incompressible fluid and the transport of discrete particulate material around obstacles impervious to flow. The numerical methods used in this code are described. SOLA-DM was used to predict the particle flux sampled by the 10-mm Dorr-Oliver Cyclone and MINIRAM dust monitors. Various geometric and dynamic variations of monitor and airflow combinations were tested. The code predictions are shown in computer-generated graphic plots.

INTRODUCTION

An improved understanding of the fluid dynamics and particulate transport as related to dust monitor sampling is desirable. The agencies concerned with monitoring respirable dust must contend with errors caused by wind velocity, sampling velocity, sampler inlet orientations, and geometric configurations. These errors, which collectively are termed "inlet bias," have been studied using mostly empirical methods. However, under the auspices of the U.S. Bureau of Mines, we have developed a computer model that simulates the airflow and particle transport around various sampling devices and then predicts the particle sampling rate.

In the second section, we describe the three-dimensional numerical method (SOLA-DM) we used. The SOLA-DM computer code solves the finite-difference approximation to the Navier-Stokes equations and the continuity equation for an incompressible fluid. The numerical model for particle transport simulates the inertial, pressure differential, drag, and body forces. In Sec. III, we describe using SOLA-DM to simulate the fluid and particle flow around the Cyclone and MINIRAM dust monitors numerically. For clarity, our discussion includes computer-generated plots of the computational mesh configuration and velocity plots of the flow field. Then, in the next section, we present the computational predictions of the sampled particle flux for the dust monitors. In the final section, we discuss the use of SOLA-DM for these calculations and make recommendations for future studies.

SOLA-DM: A THREE-DIMENSIONAL NUMERICAL METHOD

SOLA-DM (Wilson et al., 1987) is a computer code for modeling the dynamics of an incompressible fluid and the transport of discrete particulate material in three spatial dimensions. SOLA-DM is a modified version of the SOLA-3D code, which has been used (in various forms) for a variety of applications (Hotchkiss and Hirt, 1972; Nichols and Hirt, 1972; and Hirt and Ramshaw, 1976). The SOLA-DM code is described in detail in a Los Alamos National Laboratory report that is in preparation.

SOLA-DM solves the three-dimensional Navier-Stokes equations for the fluid velocity components. The differential equations are written in terms of Cartesian coordinates (x, y, and z). For cylindrical coordinates (r, θ, and z), the x coordinate is interpreted as the radial direction; the y coordinate is transformed to the azimuthal coordinate, rθ; and z is used as the axial coordinate. Several terms must be added to the Cartesian equations of motion for cylindrical geometry. The following equations include these terms by using the coefficient ξ, where ξ = 0 corresponds to Cartesian coordinates and ξ = 1 corresponds to cylindrical coordinates. The momentum equations are written as

$$\frac{\partial u}{\partial t} + u\frac{\partial u}{\partial x} + v\frac{\partial u}{\partial y} + w\frac{\partial u}{\partial z} - \xi\frac{v^2}{x} = -\frac{\partial P}{\partial x} + g_x + f_x ,$$

$$\frac{\partial v}{\partial t} + u\frac{\partial v}{\partial x} + v\frac{\partial v}{\partial y} + w\frac{\partial v}{\partial z} + \xi\frac{uv}{x} = -\frac{\partial P}{\partial y} + g_y + f_x , \text{ and}$$

$$\frac{\partial w}{\partial t} + u\frac{\partial w}{\partial x} + v\frac{\partial w}{\partial y} + w\frac{\partial w}{\partial z} = -\frac{\partial P}{\partial z} + g_z + f_z . \qquad (1)$$

The velocity components (u, v, and w) are in the coordinate directions (x, y, and z or r, θ, and z); P is the fluid pressure, p, divided by the constant fluid density, ρ; g_x, g_y, and g_z are body accelerations; and f_x, f_y, and f_z are viscous accelerations written with the constant kinematic viscosity ν (where ν = μ/ρ):

$$f_x = \nu\left[\frac{\partial^2 u}{\partial x^2} + \frac{\partial^2 u}{\partial y^2} + \frac{\partial^2 u}{\partial z^2} + \xi\left(\frac{1}{x}\frac{\partial u}{\partial x} - \frac{u}{x^2} - \frac{2}{x}\frac{\partial v}{\partial y}\right)\right].$$

$$f_y = \nu\left[\frac{\partial^2 v}{\partial x^2} + \frac{\partial^2 v}{\partial y^2} + \frac{\partial^2 v}{\partial z^2} + \xi\left(\frac{1}{x}\frac{\partial v}{\partial x} - \frac{v}{x^2} + \frac{2}{x}\frac{\partial u}{\partial y}\right)\right],$$

and

$$f_z = \nu\left[\frac{\partial^2 w}{\partial x^2} + \frac{\partial^2 w}{\partial y^2} + \frac{\partial^2 w}{\partial z^2} + \xi\left(\frac{1}{x}\frac{\partial w}{\partial x}\right)\right] . \qquad (2)$$

The mass conservation equation is expressed in terms of the continuity condition:

$$\frac{\partial u}{\partial x} + \frac{\partial v}{\partial y} + \frac{\partial w}{\partial z} + \xi\frac{u}{x} = 0 . \qquad (3)$$

The numerical solution of these equations uses a finite-difference mesh of parallelepiped cells with edge lengths of δx_i, δy_j, and δz_k, where the subscripts refer to the i^{th} cell in the x direction, the j^{th} cell in the y direction, and the k^{th} cell in the z direction. The fluid mesh region comprises IBAR cells in the x direction, JBAR cells in the y direction, and KBAR cells in the z direction. The fluid mesh region is surrounded by a single layer of fictitious cells that are used to set boundary conditions. Thus, there are usually (IBAR + 2) * (JBAR + 2) * (KBAR + 2) cells in a mesh. Using the boundary cells properly eliminates the need for special finite-difference equations at the boundaries. SOLA-DM has an automatic mesh generator that constructs a mesh of computational cells with varying spatial resolutions determined by a few input parameters.

A cycle of calculations to advance the flow configuration through a time interval, δt, consists of the following two major steps.

1. Finite-difference approximations of the momentum equations [Eqs. (1)] are used to obtain guesses for new time-level velocities based on the initial conditions or previous time-level values for all advective, viscous, pressure gradients and body acceleration terms. The new velocities will not necessarily satisfy the incompressibility condition [Eq. (2)].

2. The pressure is adjusted in each cell to ensure that the finite-difference approximation of Eq. (2) is satisfied. These pressure adjustments must be done iteratively because a change in pressure in one cell will upset the balance in neighboring cells. Suitable boundary conditions must be imposed at all mesh boundaries at each step. The number of iteration sweeps through the mesh that are needed to get a desired level of convergence to Eq. (2) in all cells varies with each problem. Typically, more iterations are required to get a problem started because large initial flow transients require large pressure adjustments. Fewer iterations are required as nearly steady flow conditions are approached. The iteration number drops to unity when steady conditions are reached.

From a mathematical point of view, the iteration process is used to obtain the solution of a Poisson equation for pressure, but this equation is not written explicitly in the code. From a physical standpoint, the pressure iteration is necessary to account for the long-range influence of rapidly propagating acoustic pressure waves that maintain a uniform density. In the original SOLA codes (Hirt et al., 1975), the pressure was adjusted for each cell (step 2 above) using a Newton-Raphson iteration. However, SOLA-DM uses the preconditioned conjugate residual method, which first was applied to a SOLA code by Daly and Torrey (Daly and Torrey, 1984). This iterative scheme as used here is described in detail in the SOLA-DM report in preparation (Wilson et al., 1987).

A complete fluid dynamics iteration cycle requires that the velocity and pressure be updated at all mesh boundaries. The mesh boundaries may be rigid no-slip, for which the normal velocity at the boundary is zero and the tangential velocity at the boundary is zero or free-slip, for which the normal velocity at the boundary is zero and the tangential velocity gradient at the boundary is zero; continuative outflow, for which the normal velocity derivative is set to zero when applying the momentum equations and the tangential velocity gradient is zero. A periodic boundary condition for any direction can be specified. A constant pressure boundary condition at any fictitious cell boundary is set by keeping the pressure constant in the layer of fluid cells adjacent to the boundary and otherwise treating the boundary as continuative outflow. Any of these boundary conditions can be imposed by setting input numbers. The user can specify in- or outflow boundary conditions in the program.

Internal mesh cells may be defined as opaque to flow. These obstacle cells are set by input numbers. All six faces of an obstacle cell have zero velocity, and the cell pressure is zero. Similarly, any set of cell faces may be specified as opaque to flow, effectively creating a thin wall.

SOLA-DM models the transport of discrete particles within the fluid mesh. The numerical model for particle transport simulates the inertial, pressure differential, drag, and body forces. In cylindrical coordinates, centrifugal force also is included. The drag force, F_D, may be defined as proportional to the product of the cross-sectional area of the particle and the dynamic pressure; that is,

$$F_D = C_D(\pi r_p^2)\left(\frac{\rho_f}{2}\right)(U_f - U_p)^2 , \qquad (4)$$

where r_p is the particle radius, ρ_f is the constant fluid density, and $(U_f - U_p)$ is the difference in the fluid and particle velocities. The drag coefficient, C_D, for flow in the Stokes region ($Re < 1.0$) is $C_D = 24/R_e$, where $R_e = (U_f - U_p)(2r_p)/\nu_f$ and ν_f is the fluid kinematic viscosity. Writing a force balance equation for a rigid spherical particle and solving for the particle acceleration in the x direction gives

$$\frac{du_p}{dt} = -\left(\frac{\rho_f}{\rho_p}\right)\frac{\partial P}{\partial x} + C_{SD}(U_f - U_p) + g_x + \omega_r^2 y , \qquad (5)$$

where

$$C_{SD} = \left(\frac{9}{2}\right)\left(\frac{\rho_f}{\rho_p}\right)\left(\frac{v_f}{r_p 2}\right) \quad , \qquad (6)$$

where v is the azimuthal fluid velocity component and r is the radius of curvature of the particle path. As noted above, $\xi = 0$ for Cartesian coordinates and $\xi = 1$ for cylindrical coordinates. This is the form of the equation used in the code. The ρ_f in the pressure differential term is present because the code "pressure" is actually fluid pressure, p, divided by the constant fluid density; that is, $P = p/\rho_f$. Equivalent equations express the particle transport in the y and z directions.

The turbulent diffusion of the dust particle is characterized by a particle diffusion coefficient, NUP. The numerical model of turbulent diffusion computes diffusion velocity components for each particle. In this model, the fluid velocity components (U_f, V_f, and W_f) at the location of each particle are the sum of the mean velocity components (linearly interpolated to the particle position from the mean velocity field) and the random turbulent velocity component. The basic idea (Hotchkiss and Hirt, 1972) in determining the random turbulent velocity is to consider the particle as a point source that diffuses for a time δt. The probability of where the particle is likely to move is given by a Gaussian distribution, with the width of the distribution determined by the standard deviation $4 \cdot \delta t \cdot$ NUP. A random number generator selects the location actually used within the distribution.

NUMERICAL SIMULATION OF PARTICULATE FLOW AROUND MONITORS

We modeled the 10-mm Dorr-Oliver nylon Cyclone respirable mass sampler and the MINIRAM personal dust monitor. They were modeled in standalone positions, that is, not mounted on a person. The Cyclone system (Cecala et al., 1983) includes a cylindrical collector, a filter, and a pump to provide a steady inlet flow rate. Our Cyclone model included only the cylindrical collector part of the system. The Cyclone was modeled with and without a 3.0-cm-diam shield around the collectors. The nylon cylinder has a 2.0 cm outside diameter and contains the sampling inlet, which has a flow area of 0.221 cm by 0.321 cm. We assumed that all particles entering this inlet were sampled.

The MINIRAM dust monitor (Lilienfeld and Stern, 1982) is fully self-contained and consists of a miniaturized light-scattering sensing configuration with passive connective flow sampling. This dust monitor is rectangular and is about 10 cm wide, 10 cm high, and 4 cm thick. The thickness is enlarged an additional 1.6 cm over a portion of the 10-cm by 10-cm monitor face by extending the sensing chamber. The sensing chamber provides a flow path for particles to move through the monitor for sampling.

The dust monitors were modeled with different coordinate systems. The circular cylinder configuration of the Cyclone monitor was represented by a cylindrical coordinate system, and the rectangular MINIRAM monitor was modeled using a Cartesian coordinate system. We modeled the 10-mm Dorr-Oliver Cyclone dust monitor assuming three planes of symmetry. Two axial planes, one through the center of the sampling inlet, were used to form a 90° section of a circular cylinder. Longitudinal symmetry about a horizontal plane through the vertical center of the inlet was assumed. These assumptions allowed a manageable finite-difference mesh size with acceptable spatial resolution. Figure 1 shows plots of x-, y-, and z-plane slices through the three-dimensional mesh of cylindrical coordinate cells. The mesh has 42 cells in the radial (x) direction, 16 cells in the azimuthal (y) direction, and 12 cells in the axial (z) direction, which is a total of 8064 computational cells. The greatest spatial resolution near the cylinder is 0.11 cm in each coordinate direction. As shown on the mesh plane plots, the mesh dimensions are 1.0 cm to 10.0 cm radially, 0° to 90° azimuthally, and 0.0 to 2.0 cm axially for the unshielded Cyclone simulations. The axial dimension was extended to 3.0 cm for the simulations using a shield that was simulated by creating a wall impervious to fluid flow at input-parameter-specified cell faces. The shield had a radius of 1.5 cm and was 1.437 cm high. The mesh cell faces specified as walls were 0.5 cm radially from the cylinder boundary. Seven cells in the z direction were used to resolve the shield height, and the cell faces specified as walls extended from 0° to 90° in the azimuthal direction. Five cells, each with a radial dimension of 0.10 cm, were used to resolve the distance between the Cyclone and the shield.

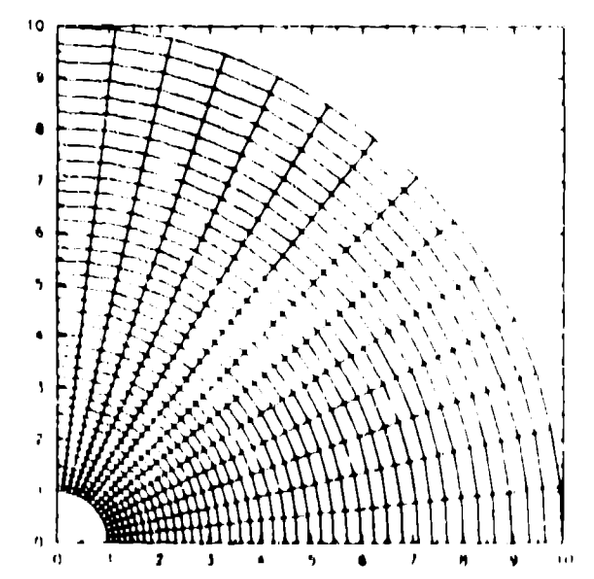

FIGURE 1(a). The cell configuration in the x y plane through the three dimensional cylindrical coordinate mesh.

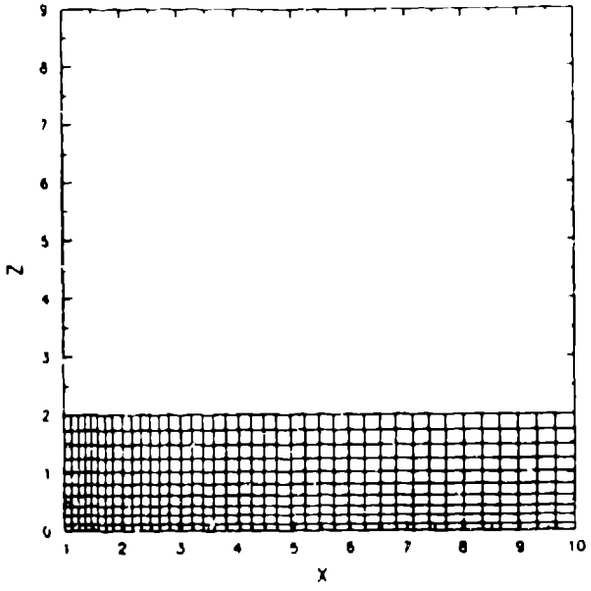

FIGURE 1(b). The cell configuration in the x-z plane through the three-dimensional cylindrical coordinate mesh.

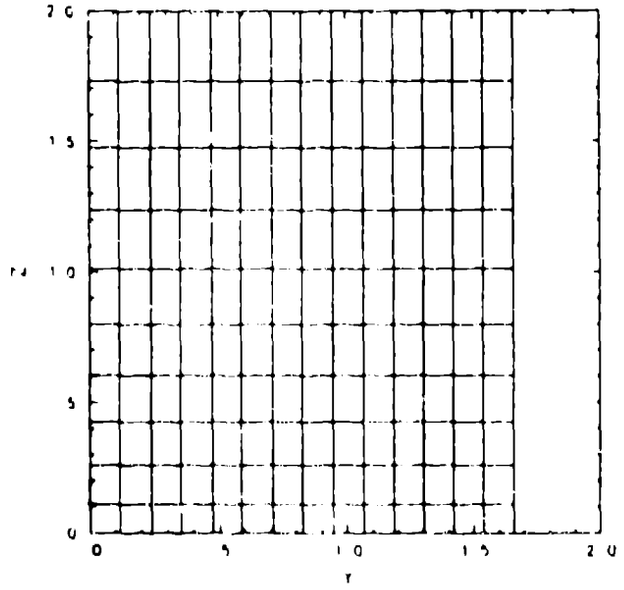

FIGURE 1(c). The cell configuration in the y-z plane through the three-dimensional cylindrical coordinate mesh.

We modeled the MINIRAM dust monitor and adjacent space using a rectangular mesh in three dimensions. A vertical plane of symmetry was assumed through the center of the monitor to reduce the number of mesh cells required. Specifically, with the monitor positioned so that the 10- by 10-cm face into which the sensing chamber is integrated is normal to the x direction, the full height (in the z direction) is modeled, but only one-half of the monitor width (in the y direction) is included in the mesh. This is possible because of the symmetry in the sensing chamber geometry and in the monitor housing. The rectangular mesh contained 43 cells in the x direction, 25 cells in the y direction, and 35 cells in the z direction, which is a total of 37 625 cells. The mesh dimensions were 0.0 cm to 30.6 cm in the x direction, 0.0 to 11.0 cm in the y direction, and 0.0 to 20 cm in the z direction. The monitor was resolved spatially by 14 cells in the x direction, 11 cells in the y direction, and 20 cells in the z direction. In the x and z directions, the monitor was approximately in the center of the mesh. The typical cell dimension in the monitor region was 0.3 cm, with the smallest dimension being 0.25 cm and the largest one being 0.38 cm. The mesh cells corresponding to the monitor were designated as obstacle cells by input parameters, and the faces of obstacle cells are impervious to flow. In Fig. 2, plots of the x, y, and z planes in the mesh show the cell configuration.

We simulated the airflow past each monitor by first setting an initial flow field in the mesh and specifying an inflow boundary condition at the mesh boundary upwind of the monitor. A continuative outflow boundary condition downwind of the monitor allows the airflow to leave the mesh with negligible upstream influence. All planes of symmetry and most of the other boundries were set as free-slip boundaries, which sets a zero normal velocity and a zero tangential velocity gradient at the boundary. However, a no-slip condition was set at the Cyclone wall. This sets a zero normal and tangential velocity at the boundary. In Fig. 3, the quasi-steady-state velocity field around the Cyclone in the x-y plane at the longitudinal plane of symmetry and the x-z plane at the 0° axial plane of symmetry is shown in a perspective view. The velocity vectors are drawn from the center of each

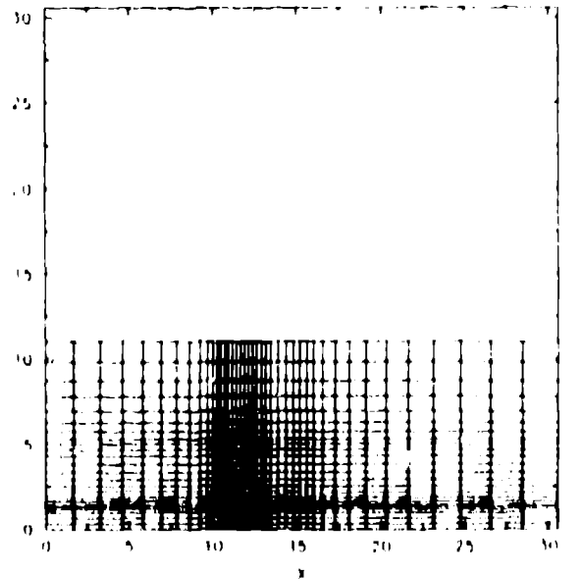

FIGURE 2(a). The cell configuration in the x-y plane through the three-dimensional cylindrical coordinate mesh.

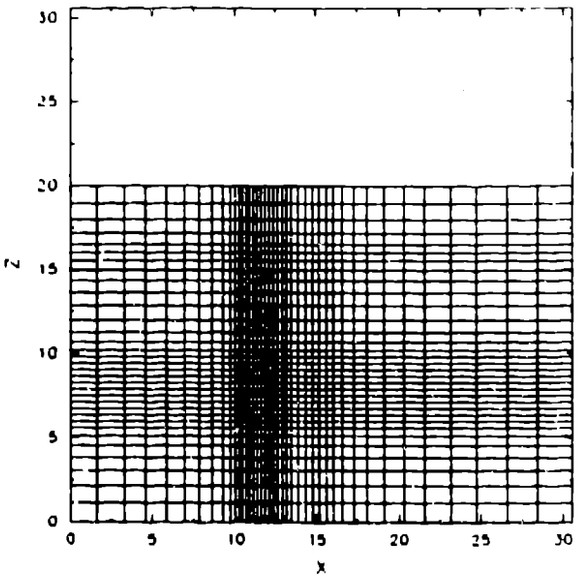

FIGURE 2(b). The cell configuration in the x-z plane through the three-dimensional Cartesian coordinate mesh.

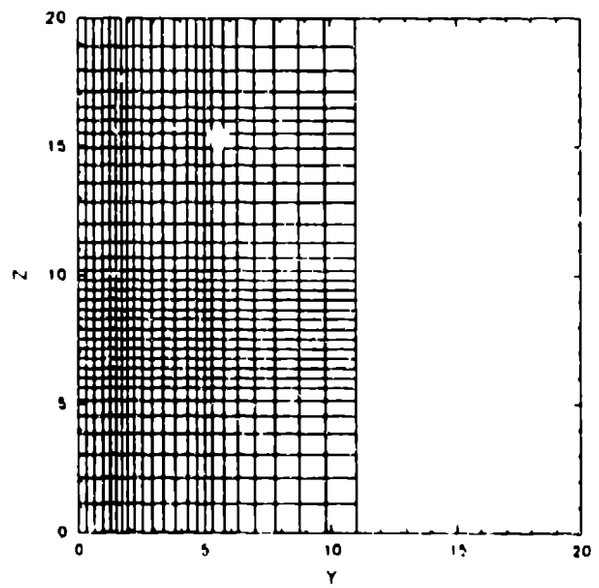

FIGURE 2(c). The cell configuration in the y-z plane through the three-dimensional Cartesian coordinate mesh.

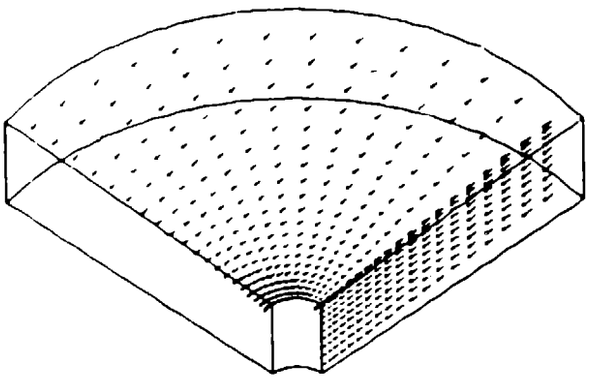

FIGURE 3. Quasi-steady-state velocity field plot in the x-y plane at the Cyclone longitudinal plane of symmetry and the x-z plane at the 0° axial plane of symmetry in perspective view.

fluid cell. The quasi-steady-state flow field around the MINIRAM is shown in Figs. 4--6. The regions without velocity vectors correspond to the location of the monitor. In Fig. 4, the flow field shown is in the x-y plane at the vertical center of the sensing volume. The flow is from the left, as indicated by the arrowheads on the vectors. The region without vectors indicates the monitor location. The expanded view in Fig. 4(b) shows the recirculation in the sensing volume in this plane. Figure 5 shows the flow field in the x-z plane at the plane of symmetry. Secondary flow again occurs in the expanded view in Fig. 5(b). The flow field in Fig. 6 is the y-z plane in the middle of the sensing volume. The expanded view in Fig. 6(b) shows the recirculating flow. The flow in the sensing volume is in three dimensions and is more complex than displayed by the slices through the region shown in the plots.

For the particle transport calculation in this study, we used a code feature that allows the user to compute the particle transport in a previously calculated quasi-steady-state fluid flow field. This eliminates the computer time required to regenerate the flow field for each particle transport case. The particle transport model does not simulate particle-particle interaction, and the particles do not influence the fluid dynamics. For these reasons, the magnitude of particle concentration is chosen to provide an adequate concentration of particles to be sampled by the monitor, but the cost of computation also must be considered. In these studies, the particle concentration input upstream of the monitor may vary from 200 particles/cm^3 for the MINIRAM simulation to 20 000 particles/cm^3 for the Cyclone simulation. The required volume of particle input is much smaller for the Cyclone. The particle transport time required by the code is about 10 μs/particle/cycle, where a cycle is the computational cycle each time step. A typical Cyclone particle transport calculation may be over a period of 50 ms, with a time step of 0.02 ms, which is 2500 cycles. At a concentration of 20 000 particles/cm^3, the total number of particles in the mesh at late times may approach 12 000. This typically requires less than 5 min on a Cray computer.

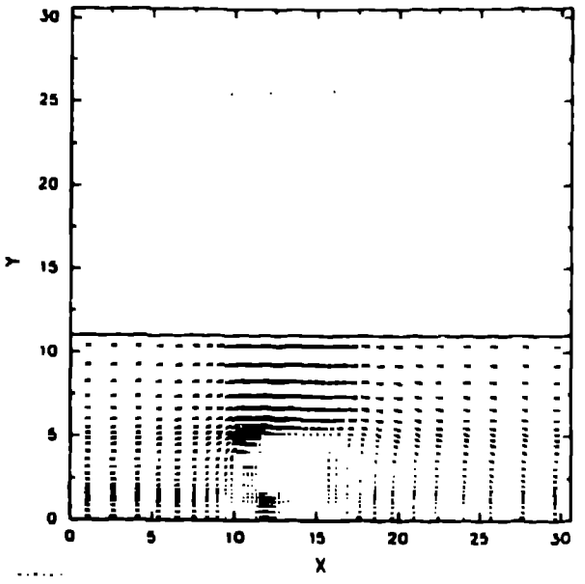

FIGURE 4(a). Quasi-steady-state velocity field plot in the x-y plane at the vertical center of the MINIRAM monitor sensing volume.

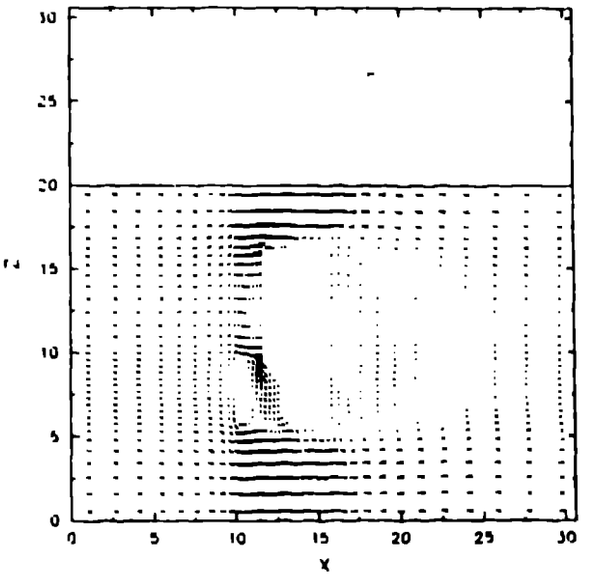

FIGURE 5(a). Quasi-steady-state velocity field plot in the x-z plane at the vertical plane of symmetry of the MINIRAM monitor.

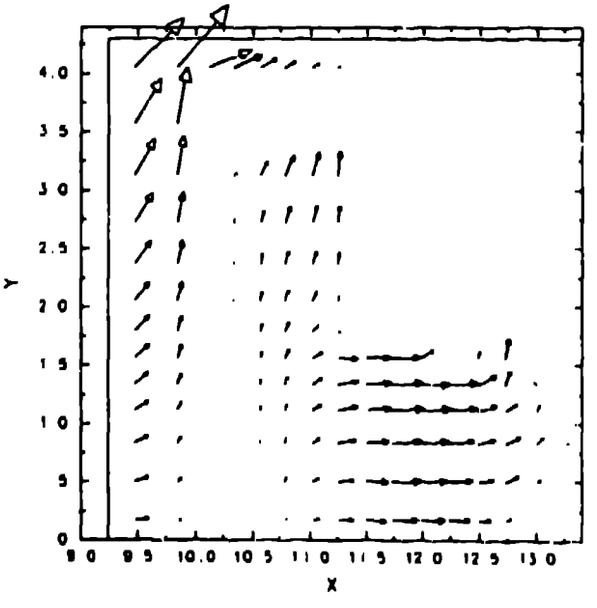

FIGURE 4(b). Expanded view of the velocity field in the x-y plane at the vertical center of the MINIRAM monitor sensing volume.

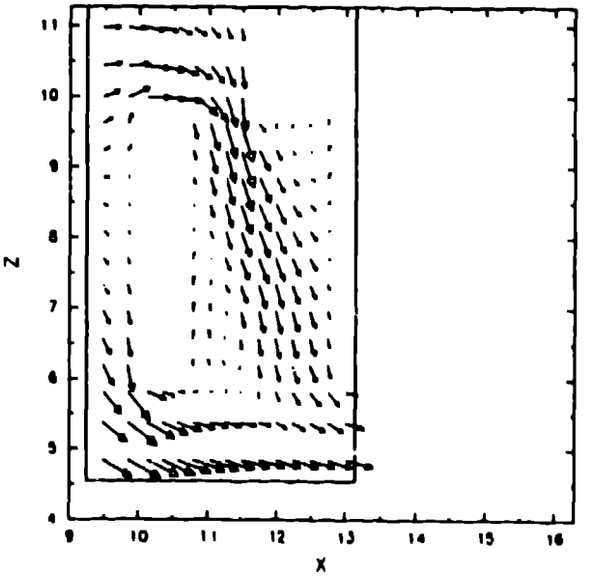

FIGURE 5(b). Expanded view of the velocity field in the x-z plane at the vertical plane of symmetry of the MINIRAM monitor.

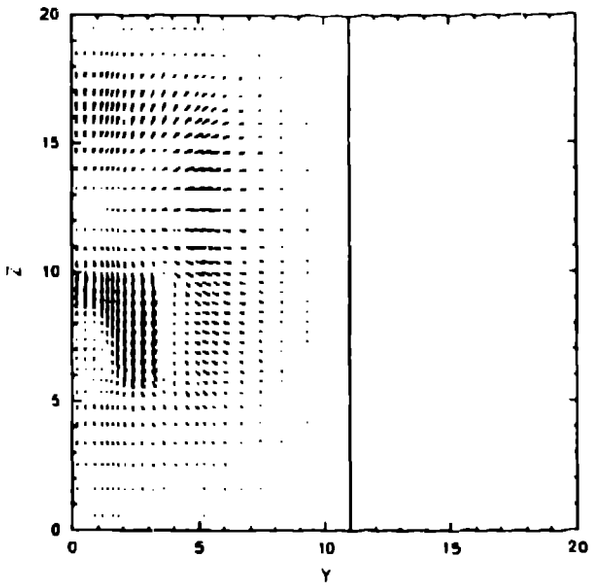

FIGURE 6(a). Quasi-steady-state velocity field plot in the y-z plane at the approximate middle of the MINIRAM monitor sensing volume.

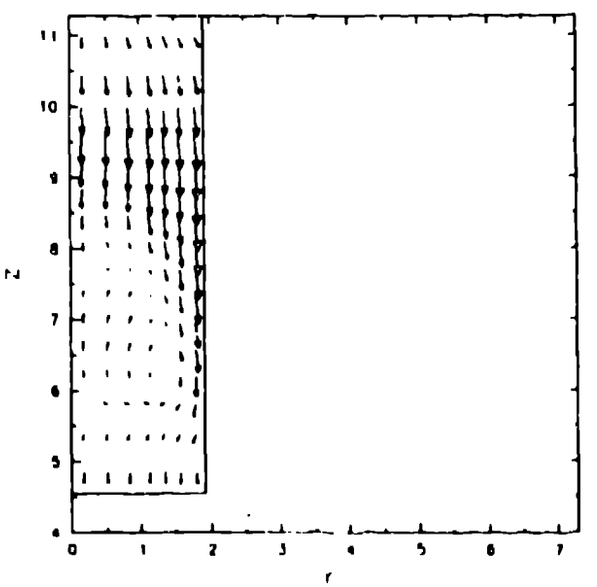

FIGURE 6(b). Expanded view of the velocity field in the y-z plane at the approximate middle of the MINIRAM monitor sensing volume.

SOLA-DM PREDICTIONS OF SAMPLED PARTICLE FLUX

To study their effects on the Cyclone particle sampling rates, we varied the monitor orientation, the particle size, the wind speed, the sampling flow rate, and the effect of a shield around the inlet. The Cyclone inlet was oriented to face directly into the wind at 0° or perpendicular to the wind at 90°. Each of the simulations was run with three particle sizes (aerodynamic diameters): 0.1 μm, 1.0 μm, and 10.0 μm. We used wind speeds of 152.4 and 406.4 cm/s and specified the sampling flow rates as 1.2 and 2.0 L/min. A shield was placed around the cyclone inlet that extended radially 0.5 cm beyond the Cyclone and was 1.437 cm long.

The code simulations predicted that, of the conditions modeled, the greatest effect on the Cyclone sampling rate was the orientation of the monitor relative to the wind direction. In the simulation of the unshielded Cyclone with an inlet flow rate of 2.0 L/min and a wind speed of 152.4 cm/s, the predicted average particle flux of all the particle sizes sampled at the 90° orientation is only 31% of the particle flux at a 0° orientation. The average particle flux data for high wind speed (406.4 cm/s) indicate virtually the same reduction in particle flux for a change in orientation from 0° to 90°. The code predicted that the shield reduces the effect of orientation on sampling rate. The sampling rate for the shielded Cyclone at 90° is 48% of the sampling rate at 0°. Although the magnitudes differ, the inlet sampling rates increase about the same percentage from low to high wind speed for the 0° and 90° orientation to the wind direction for the unshielded simulations. At a 0° orientation, a 67% increase in the inlet flow rate increased the average particle flux by 71%.

At a 0° orientation, the predicted effect of adding the 1.5-cm radius shield around the 1.0-cm-radius Cyclone monitor was a reduction in sampling rate for all particle sizes by 3%. However, at a 90° orientation, the code predicted an increase of 71% from unshielded to shielded simulations. These results indicate that the particle inertia strongly affects the predicted sampling rate.

The 10-μm-diam particles were not collected under any of the cases that were simulated. A conservative analysis, described in Ref. 1, suggests that these large-diameter particles moved away from the Cyclone boundary area because of centrifugal force. However, it is not understood why the shielded, 90° orientation simulation predicted zero particle flux.

The MINIRAM monitor simulations were for one orientation and wind speed. Particles with aerodynamic diameters of 0.10, 1.68, 3.36, 16.8, and 33.6 μm were modeled. We computed the percentages of the free-stream particle concentrations that flow through the MINIRAM sensing volume. The sensing volume corresponds to the MINIRAM scattering volume defined by the intersection of the solid angles formed by the light passing through the focusing lenses of the light source and the light detector. The sensing volume is modeled in the code

by estimating the number of cells and the portions of cells included in the intersection of these solid angles.

The predicted particle concentration in the sensing volume is affected by the size of the particle. The percentage of free-stream concentration varies from 90% for 0.1-μm-diam particles to only 60% for the rather large 33.6-μm-diam particles. In our numerical model, this difference can be understood by noting the number of particles in each computational cell in the sensing chamber. The larger particles are concentrated near the rear (downstream side) of the sensing chamber, which only partially coincides with the sensing volume. Consequently, the total count in the sensing volume is less than that for the more evenly distributed smaller particles. We made another measurement that makes this observation even more obvious. The probe used in an experimental study of dust flow around and through the MINIRAM by Asay and Hull (Asay and Hull, 1986) was located near the front (upstream side) of the sensing volume. To compare the numerical predictions with the experimental measurements of concentration, we counted the particles at the approximate probe location. The particle concentrations were 95%, 94%, 73%, 49%, and 10% of the free-stream values for the respective particle aerodynamic diameters of 0.1 μm, 1.68 μm, 3.36 μm, 16.8 μm, and 33.6 μm. The concentrations at the probe location and in the sensing volume are within a few per cent of each other for the smaller particles but vary 28% to 50% for the particles greater than 10 μm. The larger particles probably migrate to the back (downstream) side of the monitor sensing region because of their downstream inertia as they enter the downward-turning flow in the top section of the sensing chamber.

CONCLUSIONS

The SOLA-DM computer code is well suited to perform the simulations in this study. The code's solution algorithm is especially efficient with the use of the preconditioned conjugate residual iteration method, which allows rapid convergence to an accurate solution for the pressure field. The SOLA-DM user's manual and the code's internal documentation make the code easy to use. These studies were simplified by generating the flow field only once for each configuration and then injecting particles into the system. In this way, the parameters controlling the particle behavior could be evaluated easily.

The SOLA-DM code predicts that the factor having the largest effect on the Cyclone monitor sampling rate is the monitor orientation relative to the wind direction. This is the case for both of the wind speeds simulated, but this effect is moderated by the addition of the shield. As expected, the sampling rate for the 0° orientation is increased for an increase in the wind speed. The same pattern is true for the 90° orientation, which was not expected. At a 0° orientation, the sampling rate was proportional to the inlet flow rate. Several of the simulations indicated that particle inertia, and consequently particle size, affect the Cyclone sampling rate. This effect is especially notable for the 90° orientation because in no case was the 10-μm-diam particle collected. The approximate analysis of particle motion around a cylinder may explain this; however, the shield was expected to have a greater effect on the particle behavior near the Cyclone than was predicted.

The MINIRAM monitor simulations indicate that particle size is a major factor in particle concentration in the sensing volume. The value of the particle diffusion coefficient also influences the distribution of particles in the sensing chamber. The value of 10.0 cm^2/s seemed to be a good estimate, but additional attention should be given to this parameter.

REFERENCES

Asay, B. W. and Hull, L. M., 1936, "An Experimental Investigation of Particulate-Laden Inner Airflow Around a Personal Dust Monitor," LA-UR-86-645, Los Alamos National Laboratory.

Cecala, A. B., Volkwein, J. C., Timko, R. J., and Williams, K. L., 1983, "Velocity and Orientation Effects on the 10-mm Dorr-Oliver Cyclone," Report of Investigation 8764, U.S. Bureau of Mines.

Daly, B. J. and Torrey, M. D., 1984, "SOLA-PTS: A Transient, Three-Dimensional Algorithm for Fluid-Thermal Mixing and Wall Heat Transfer in Complex Geometries," LA-10132-MS, NUREG/CR-3822, Los Alamos National Laboratory.

Hirt, C. W., Nichols, B. D., and Romero, N. C., 1975, "SOLA - A Numerical Solution Algorithm for Transient Fluid Flows," LA-5852, Los Alamos Scientific Laboratory.

Hirt, C. W. and Ramshaw, J. D., 1978, "Prospects for Numerical Simulations of Bluff Body Aerodynamics," Aerodynamic Drag Mechanisms of Bluff Bodies and Road Vehicles, Souran, G., Morel, T., and Mason, W. J. Jr., Eds., Plenum Publishing Corporation, New York.

Hotchkiss, R. S. and Hirt, C. W., 1972, "Particulate Transport in Highly Distorted Three-Dimensional Flow Fields," in Proceedings Computer Simulation Conference.

Lilenfeld, P. and Stern, R., November 1982, "Personal Dust Monitor - Light Scattering," mining research report for contract No. H0308132, U.S. Bureau of Mines.

Nichols, B. D. and Hirt, C. W., 1973, "Transient Three-Dimensional Fluid Flow in the Vicinity of Large Structures," in Proceedings Third International Conference on Numerical Methods in Fluid Mechanics, Lecture Notes in Physics 19, Ehlers, J., Hepp, K., and Weidenmuller, H. A., Eds., Springer-Verlag, New York, Vol. II, pp. 206-213.

Wilson, T. L., Nichols, B. D., Hirt, C. W., and Stein, L. R., 1987, "SOLA-DM - A Numerical Solution Algorithm for Transient Three-Dimensional Flows," report in preparation, Los Alamos National Laboratory.